The wet corrosion of Mo and Mo-Ti alloy thin film – Part IV: The effect of nitriding

C.R. Tomachuk, D.B. Mitton, J. Springer, T. Monetta and F. Bellucci*

A considerable number of detailed investigations have been carried out on the deposition and characterisation of molybdenum and molybdenum-titanium-nitride films by employing a variety of techniques. However, very little is currently known about the effect of composition (N_2/Ar flow rate) on the corrosion properties of MoN and MoTiN thin films for aggressive ambient conditions. In this work, the electrochemical and corrosion behaviour of MoN and MoTiN thin films, produced by Physical Vapour Deposition (PVD) with different N_2/Ar flow rates, has been investigated by Electrochemical Impedance Spectroscopy (EIS) in aerated alkaline chloride solution and compared with the behaviour of pure molybdenum in the same environment. Results obtained indicate that increasing nitrogen content in the film leads to a beneficial effect on the corrosion resistance, but results in decreased electrical conductivity of the film that may limit their application as back contact in photovoltaic modules.

1 Introduction

The transition metal nitrides can be prepared as thin films or coatings by several techniques such as: (i) chemical vapour deposition (CVD) [1, 2], (ii) physical vapour deposition (PVD) [3], (iii) arc-physical vacuum deposition [4], (iv) microwave plasma [5], (v) magnetron sputtering [6–9], (vi) multipulse laser irradiation [10, 11] and, (vii) ion implantation [12].

Recently, PVD of thin film onto various substrates has been the most popular technique for obtaining molybdenum and molybdenum nitride. The advantage of this technology includes the fact that these films are easily and reproducibly formed by magnetron sputtering or reactive magnetron sputtering from a pure Mo target in an Ar or an Ar-N_2 gas mixture [9]. *Hoffmann* [13] was the first to make a systematic study of the formation of nitrides by sputtering titanium, molybdenum, niobium and zirconium targets in Ar/N_2 mixtures.

Mo and molybdenum nitride thin films have been extensively used in various technological areas, due to their remarkable properties such as high hardness, high brittleness, high melting point, high superconductivity transition temperature in several of these compounds, good chemical stability [14, 15], wear and corrosion resistance [4], and catalytic properties [16].

During a study of the tribological properties of MoN, results indicated that increasing nitrogen content in the film provides a beneficial effect on the tribological performance (hardness and wear properties) [4]. *Valli* et al. [17], and *Truman* et al. [18], showed an enhancement of pitting corrosion after the addition of N into the alloy. The greatest effect of nitrogen has been observed in molybdenum bearing stainless steels, suggesting a synergism between molybdenum and nitrogen [19, 20]. *Levis* [21] and *Papaconstantopoulos* [14] studied the electronic and mechanical properties in transition metal nitrides.

The interesting physical properties of thin films of transition metal compounds have made them extremely useful for such applications as wear and corrosion resistance coating and diffusion barriers in semi-conductor metallization. *Anitha* et al. discussed the possible use of γ-Mo_2N thin film as a diffusion barrier layer in Si-based microelectronic devices to prevent the interdiffusion or reaction of the contact metal with the substrate silicon, and as a hard coating material (on machining tools and turbine blades) [7, 8, 22].

Lu et al. [23] observed the effect of nitriding on the anodic behaviour of molybdenum. The formation of nitrides on the surface of anodically polarized stainless steel inhibits transpassive dissolution of Mo and effectively retains molybdenum in the passive surface, thereby enhancing passivity.

Oxidation properties of several nitride coatings, especially TiN, CrN and TiAlN have been extensively investigated. *Solak* et al. [3], studied the oxidation behaviour of MoN coatings by employing gravimetric tests. They observed that the oxidation resistance of MoN coatings is poor as a result of their non-protective nature and the volatility of the oxides at moderately high temperatures.

Nagae et al. [24] investigated nitriding of diluite Mo alloys (containing 0.5 wt% Ti) and observed that the inward diffusion of nitrogen is a rate-controlling process in the growth of the surface nitriding layer. In MoTi alloy an additional internal nitriding layer, with relatively high hardness, was formed beneath the surface nitriding layer.

* *F. Bellucci, T. Monetta*
Dipartimento di Ingegneria dei Materiali e della Produzione, Università degli Studi di Napoli „Federico II“
P.le Tecchio, 80, 80125, Napoli (Italy)
E-mail: bellucci@unina.it

C.R. Tomachuk
Divisão de Corrosão e Degradação, Instituto Nacional de Tecnologia
Av. Venezuela, 82 sala 608, CEP 20081-312, Rio de Janeiro, RJ (Brasil)

D.B. Mitton
Engineered Surfaces Center, University of North Dakota
P.O. Box 8155, 243 Centennial Drive, Grand Forks, ND 58202-8155 (USA)

J. Springer
Zentrum für Sonnenenergie und Wasserstoff-Forschung, Baden-Württemberg
70565 Stuttgart (Germany)

The preparation and investigation of molybdenum nitride (MoN) and molybdenum-titanium nitride (MoTiN) thin films are not as extensive as other transition metal nitrides such as titanium nitrides. Moreover, the effect of N_2/Ar flow rate on the corrosion properties of MoN and MoTiN thin films remains essentially unexplored.

During the present investigation, the effect of N_2/Ar flow rate on the corrosion properties of MoN and MoTiN thin films obtained by PVD was studied by both dc and ac techniques in an aerated chloride solution at pH 12.

An aerated alkaline solution was selected for the following two reasons: (a) previous research indicated that Mo corrosion is more severe at a higher pH value [25, 26], and (b) the high pH solution more closely resembles the microenvironment of undercoating corrosion. Therefore pH 12 can be considered as the most suitable for studying undercoating corrosion and the most aggressive for Mo alloy thin films.

2 Materials and methods

2.1 Samples

Thin films samples used in this investigation were deposited onto a glass substrate 3×3 cm^2 by Zentrum für Sonnenenergie und Wasserstoff-Forschung (ZSW), Stuttgart, Germany, employing a PVD technique conducted under proprietary conditions. The argon and nitrogen ratio was varied to form MoN and MoTiN alloys of different composition. The electrical resistivity of these films was calculated by measuring the electrical resistance and the film thickness obtained through profilometer. These values are reported in Table 1. A pure Mo thin film was used as a standard reference sample for comparative purposes.

2.2 Test solution

In all cases, the electrolyte was aqueous aerated 0.6N NaCl solution at pH 12. The pH adjustment was accomplished by the addition of sodium hydroxide solution.

2.3 Electrochemical behaviour

A systematic study of the corrosion behaviour of MoN and MoTiN thin film samples in the test solution was undertaken using both dc and ac techniques.

In all cases, an electrochemical cell was produced by sealing a glass cylinder onto the working electrode by means of an O-ring. This formed an exposed sample surface area of 3.14 cm^2. The reference electrode employed was Ag/AgCl and a platinum counter electrode was used in all cases. Throughout this paper, all electrochemical potentials are referenced to the Saturated Calomel Electrode (SCE).

The potentiodynamic polarisation curves were performed at a scan rate of 1 mV/s in the range from −0.300 V (SCE) at –2.000 V (SCE) relative to the ocp. Electrochemical Impedance Spectroscopy (EIS) measurements were performed in the frequency range 10^{-2} Hz-10^{-5} Hz using a Solartron 1260 Frequency Response Analyzer (FRA) in combination with a Solartron 1286 electrochemical interface, and a superimposed sinusoidal voltage signal of 5 mV. The experimental spectra were interpreted on the basis of equivalent electrical circuits using ZView fitting software by Scribner Associates. All measurements were carried out in a Faraday cage in order to minimize external interference on the system studied.

2.4 Thickness measurements

The thickness of the samples was measured using Helmut Fischer equipment Dualscope MP4.

3 Results and discussion

Samples of MoN, and MoTiN thin films, were prepared at ZSW in a semi-continuous sputtering reactor by varying the N_2/Ar flow ratio as reported in Table 1. A pure Mo thin film sample (S1) was used as the reference standard.

Figs. 1 and 2 present the sheet resistance in Ωcm^2 and the film thickness, in nm, as a function of the N_2/Ar ratio. It is apparent from these figures, that an increase of N_2/Ar flow ratio during deposition, results in reduced thickness and increased resistance of the film. The increased film resistance could lead to a decrease in the collecting efficiency of the back contact. The reduction of film thickness shown in Fig. 2 indicates a lower efficiency during deposition (considering constant deposition time) as the N_2/Ar flow ratio increases. These data are in agreement with those reported by *Mientus* et al. [27].

3.1 Potentiodynamic polarisation measurements

Figs. 3 and 4 present the potentiodynamic polarisation curves obtained for MoTiN and MoN thin film samples, respectively. Pure Mo was used as a standard reference. The curves presented in Figs. 3 and 4 exhibit similar features. By increas-

Table 1. Composition, properties and thickness of the samples furnished by ZSW

Identification	Composition	N_2/Ar Flow ratio	Sheet resistance (Ωcm^2)	Thickness (nm)
S1	Mo 100% (ref.)	0	0.50	≈ 300
S2	(MoTi)Nx	0.2	4.8	≈ 280
S3	(MoTi)Nx	0.5	7.8	≈ 240
S4	(MoTi)Nx	1.0	11.8	≈ 200
S5	MoNx	0.05	0.50	≈ 300
S6	MoNx	0.10	0.84	≈ 290
S7	MoNx	0.15	1.19	≈ 280
S8	MoNx	1.0	5.17	≈ 220

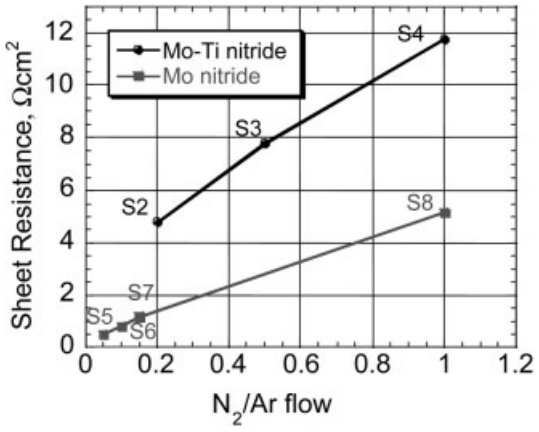

Fig. 1. Plot of the sheet resistance as a function of N_2/Ar flow ratio for samples analysed

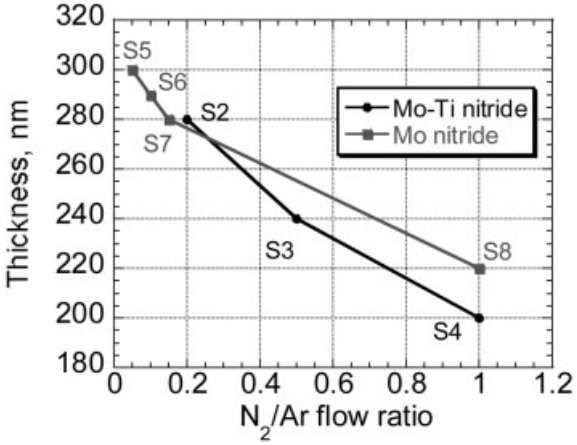

Fig. 2. Plot of the thickness as a function of N_2/Ar flow ratio for samples analysed

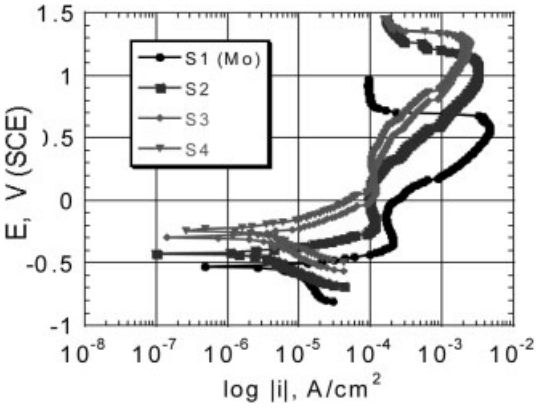

Fig. 3. Polarisation curves for pure molybdenum and Mo-Ti nitride thin film samples in aqueous aerated 0.6N NaCl solution, pH 12, at 25 °C. Sweep rate of 1 mV/s

ing the potential above the ocp, pseudopassivity followed by anodic dissolution is observed with an abrupt decrease in the anodic current at higher voltages. The latter result was attributed to the substantial dissolution of the film with subsequent loss of contact with the electrochemical instrumentation.

During anodic polarisation in the aerated alkaline chloride solution, the colour of the electrode changed from metallic

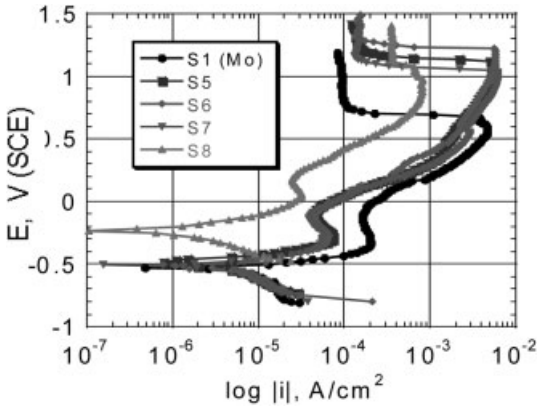

Fig. 4. Polarisation curves for pure molybdenum and molybdenum nitride thin film samples in aqueous aerated 0.6N NaCl solution, pH 12, at 25 °C. Sweep rate of 1 mV/s

silver to brown in the pseudopassivity potential range. At more positive potentials, concurrent with the rapid dissolution of the film, the test solution changed from colourless to blue. Similar results were observed by others for acidic electrolytes at high current densities [28].

By assuming Tafel behaviour, an estimate of the corrosion current for each sample in the test solution was obtained. These values, together with the corrosion potential, E_{corr}, are reported in Table 2 and represented in Figs. 5 and 6 as a function of N_2/Ar flow rate. As shown in Fig. 5, the corrosion potential, E_{corr}, shift in the noble direction by increasing the N_2/Ar flow ratio. This result suggests better protective properties of the oxides formed on MoTiN and MoN compared to that exhibited by the pure Mo sample (S1). As can be seen from the data presented in Fig. 6, the MoN and MoTiN thin films exhibited a reduction in the corrosion rate as the N_2/Ar flow rate increased. In addition, the corrosion rate of the alloys is lower than that of pure Mo as reported in Table 2.

3.2 EIS measurements

The evaluation of the reliability of the thin films was performed with EIS. Measurements were carried out in the test solution at room temperature, and terminated upon observation of a macroscopic blue surface colour. Bode impedance modulus and phase angle diagrams at different times of exposure are shown in Figs. 7 to 14.

Table 2. Electrochemical characteristic to the samples in aqueous aerated chloride solution

Identification	E_{oc} V(SCE)	E_{corr} V(SCE)	I_{corr} (μA/cm^2)
S1	− 0.52	− 0.53	6.7
S2	− 0.40	− 0.42	2.2
S3	− 0.27	− 0.31	2.1
S4	− 0.20	− 0.25	1.4
S5	− 0.44	− 0.48	3.9
S6	− 0.46	− 0.53	3.5
S7	− 0.47	− 0.50	3.5
S8	− 0.20	− 0.24	1.3

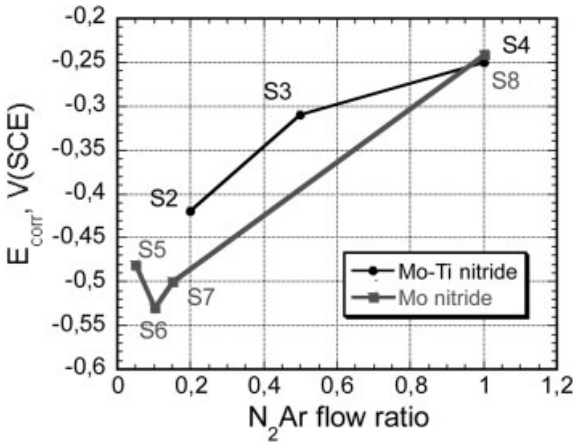

Fig. 5. Plot of the corrosion potential as a function of N_2

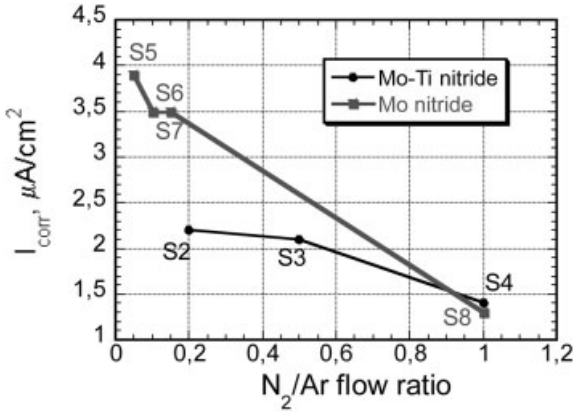

Fig. 6. Plot of the corrosion current density as a function of N_2

3.2.1 Pure Mo sample

Fig. 7 shows the Bode and phase angle spectra as a function of frequency at various exposure times in the test solution for the pure Mo, sample S1, up to the time of its complete dissolution, which occurred 9 days after initiating the test.

It is apparent from Fig. 7 (a) that the pure Mo sample (S1), exhibits resistive behaviour at high and medium frequencies (between 10^4 Hz and 10^2 Hz) upon immersion in the test solution (time $t = 0$). The impedance modulus value is about $10^2\ \Omega cm^2$. At the medium and low frequencies (between 10 Hz and 0.1 Hz) the sample exhibits pseudocapacitive behaviour, with a $|z|$ value of about $2 \times 10^3\ \Omega cm^2$ at 0.1 Hz. At very low frequencies, (between 0.1 Hz and 0.02 Hz), a new resistive region with an impedance modulus value of about $3 \times 10^3\ \Omega cm^2$ appears.

This behaviour is confirmed by the phase angle data in Fig. 7(b). At an exposure time of zero for sample S1, a phase angle value of zero is observed between 10^4 and 10^2 Hz, (corresponding to the resistive region at high and medium frequencies seen in the Bode plot), while a maximum value of about 62 ° is observed at 1 Hz. A decrease of the phase angle is again observed in the very low frequency range.

With increasing exposure time, both the Bode and phase angle plots for sample S1 reveal changes. As far as the resistive region at high and medium frequencies is concerned, a slight increase with time is observed with a final value of $2 \times 10^2\ \Omega cm^2$ after 9 days. Simultaneously, regions of sample S1 exhibited partial dissolution. The pseudocapacitive region exhibited significant changes with immersion time characterized by a progressive increase of the frequency range in which the behaviour is visible. In addition, the impedance modulus value calculated at the same frequency decreases with exposure time.

For example, at 1 Hz, the $|z|$ value decreases from $6 \times 10^2\ \Omega cm^2$ at time zero, to about $2 \times 10^2\ \Omega cm^2$ after 2 days of exposure. At very low frequencies (0.02 Hz), it is possible to observe an increase of the $|z|$ value with time. At time zero, this value is about $4 \times 10^3\ \Omega cm^2$ while, after three hours of exposure it increases to $9 \times 10^3\ \Omega cm^2$. The phase angle variation as a function of frequency at various exposure times for sample S1, is presented in Fig. 7(b). As can be seen from this figure, a shift to the left of the phase angle in the high frequency range is observed after two days of immersion in the test solution. This behaviour is, however, accompanied by an increase of the maximum phase angle value to approximately 80 ° after 1 day of exposure. This result likely reflects the development of a layer of corrosion products on the surface of the sample that separate the substrate thin film Mo from the aggressive environment. During extended immersion, a further shift to lower frequencies is observed with a reduction of the corresponding values of the phase angle. This result can be attributed to an increase in defects in this layer with subsequent further degradation of the thin film. The maximum value of the phase angle decreases from 80 ° after one day to approximately 65 ° after 9 days.

3.2.2 MoTiN samples

Figs. 8, 9 and 10 show the impedance spectra and phase angle with exposure time for the MoTiN sample obtained with a N_2/Ar flow ratio of 0.2 (sample S2), 0.5 (sample S3) and 1.0 (sample S4).

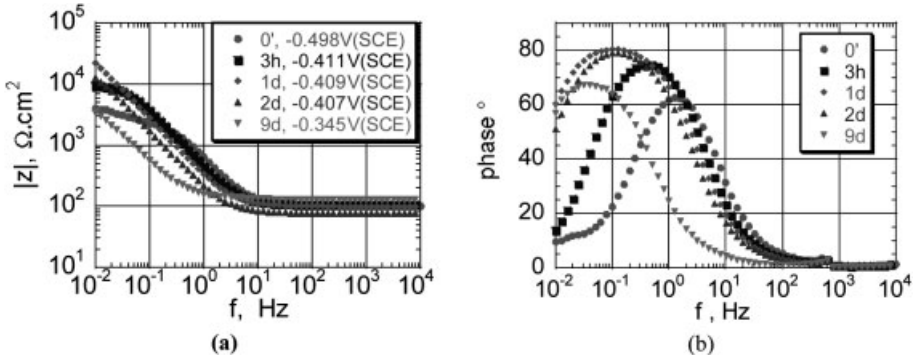

Fig. 7. Bode plot (a) and phase angle (b) as a function of immersion time in aqueous aerated 0.6N NaCl solution at pH 12, for pure molybdenum sample (S1)

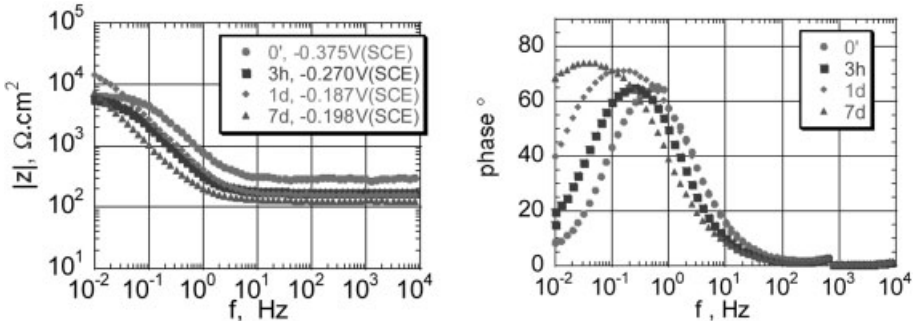

Fig. 8. Bode plot (a) and phase angle (b) as a function of immersion time in aerated 0.6N NaCl solution at pH 12, for $(MoTi)N_x$ sample, with $x = 0.2$ (S2)

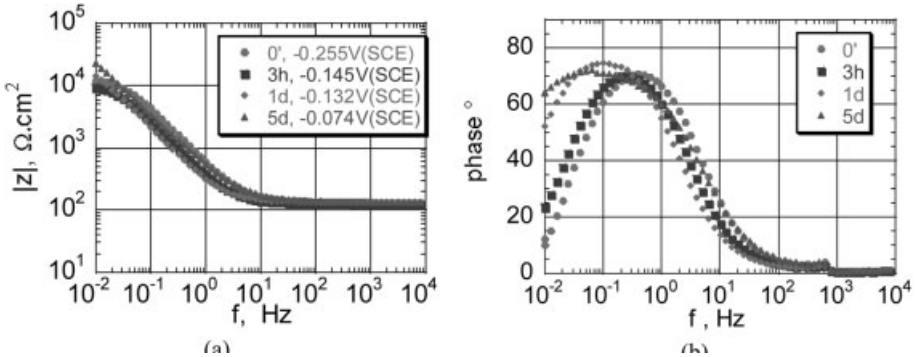

Fig. 9. Bode plot (a) and phase angle (b) as a function of immersion time in aerated 0.6N NaCl solution at pH 12, for $(MoTi)N_x$ sample, with $x = 0.5$ (S3)

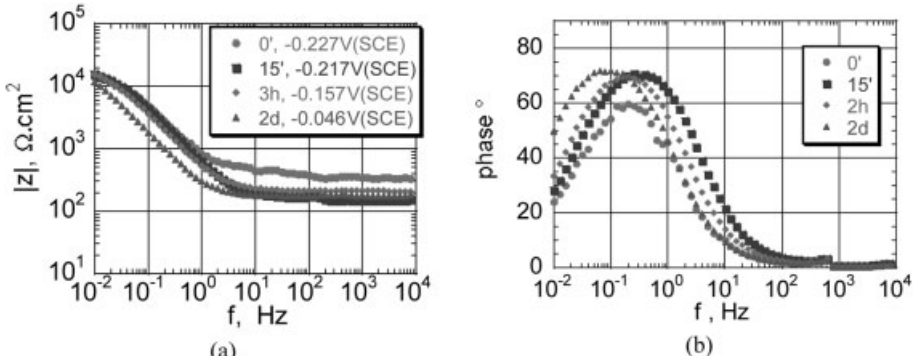

Fig. 10. Bode plot (a) and phase angle (b) as a function of immersion time in aerated 0.6N NaCl solution at pH 12, for $(MoTi)N_x$ sample, with $x = 1.0$ (S4)

Sample S2 dissolves in seven days of exposure to the test solution. For this sample, it is also possible to observe at exposure time zero, both in the impedance spectra and in the phase angle plot, a resistive region at high and medium frequencies, a pseudocapacitive region at medium and low frequencies and a resistive region at very low frequencies.

The impedance modulus at high and medium frequencies for S2 is higher then that for the S1 sample with a value of about $3 \times 10^2\ \Omega cm^2$. Furthermore, it can be observed, from the phase angle plot, that sample S2 exhibits high phase angle values at all frequencies suggesting improved dielectric properties of the air formed oxide. With increasing exposure time, the high frequency impedance of this sample decreases to a value on the order of $2 \times 10^2\ \Omega cm^2$ while fluctuations of the phase angle are observed up to 7 days of immersion in the medium frequency range (Fig. 8(a) and (b)).

Figs. 9 and 10 present the impedance spectra and the phase angle data at various exposition times for the MoTiN thin film obtained with a flow rate N_2/Ar equal to 0.5 (S3 sample) and 1.0 (S4 sample), respectively.

It was experimentally observed that sample S3 dissolved after exposure for five days, while sample S4 dissolved after only two days. For samples S3 and S4, at time zero, the z value at low frequency (0.02 Hz) is high with respect to S2 and S1. The variation of modulus of impedance and phase angle with immersion time during the test, suggest these samples are more stable. Further, 15 min after immersion, sample S4 exhibits a shift of phase angle toward higher frequency. This was followed subsequently by a shift toward lower frequencies during prolonged immersion. This result suggests a better dielectric behaviour of the corrosion products formed on the surface of this sample, followed subsequently, by time dependent degradation.

Qualitatively, upon initial immersion, S4 presents the lowest corrosion rate followed by S3, S2 and S1, respectively. This behaviour is in agreement with the results obtained from the polarisation curves.

In the following section, the behaviour of MoN samples will be examined and discussed.

3.2.3 MoN samples

In Figure 11(a), the impedance spectra shows resistive-capacitive-resistive behaviour for sample S5. Initially, the $|z|$ value at low frequency (0.02 Hz) is on the order of $7 \times 10^3\ \Omega cm^2$; however, this decreases with time. After 1 day, only one capacitive contribution was observed.

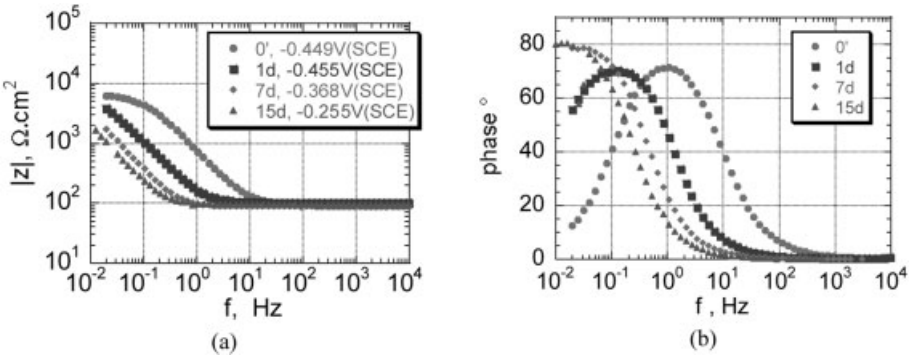

Fig. 11. Bode plot (a) and phase angle (b) as a function of immersion time in aqueous aerated 0.6N NaCl solution at pH 12, for MoN_x sample, with $x = 0.05$ (S5)

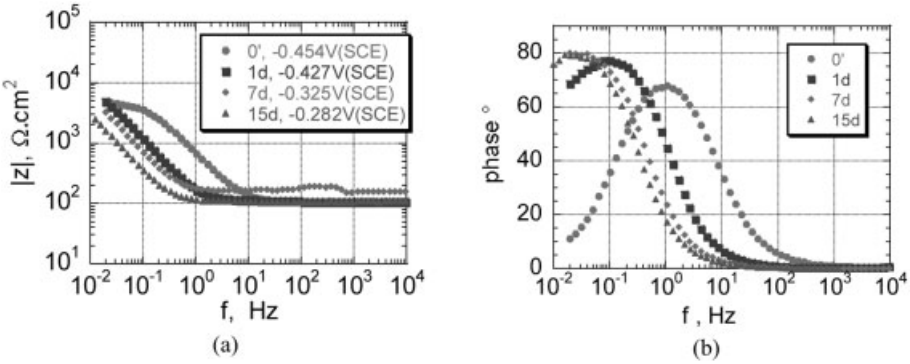

Fig. 12. Bode plot (a) and phase angle (b) as a function of immersion time in aqueous aerated 0.6N NaCl solution at pH 12, for MoN_x sample, with $x = 0.10$ (S6)

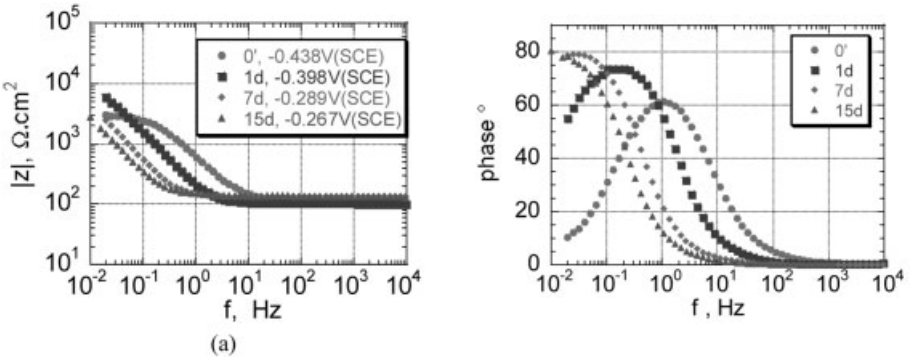

Fig. 13. Bode plot (a) and phase angle (b) as a function of immersion time in aqueous aerated 0.6N NaCl solution at pH 12, for MoN_x sample, with $x = 0.15$ (S7)

Fig. 11(b), shows one time constant with a maximum around 70 °, that shifted to lower frequencies after 1 day of exposure. After 7 days of exposure, the phase angle reached about 80 ° and a visual change in the colouration of the surface of the sample, suggesting oxide film formation, was seen. Initially, sample S5 performs better than pure Mo as can be seen by comparing data of Fig. 11 with those of pure Mo (Fig. 7) suggesting a beneficial effect of N on the short term corrosion behaviour of pure Mo.

Data presented in Figs. 12 and 13 for sample S6 and S7, do not reveal improved corrosion resistance at short exposure time. However, at longer time, these samples exhibit better corrosion performance compared to pure Mo, suggesting a beneficial effect from increasing the N_2/Ar flow rate.

In Fig. 13(a), the impedance spectra at time zero shows capacitive-resistive behaviour, with impedance modulus values, at low frequency, on the order of $3 \times 10^3\ \Omega cm^2$. After 1 day of exposure, only one capacitive contribution was observed and the impedance modulus values, at low frequency, increased to $7 \times 10^3\ \Omega cm^2$. Fig. 13(b), shows one time constant with maximum around 60 °, that after 1 day of exposure shifted to lower frequencies with a maximum of about 80 °. No major differences were observed with subsequent exposure to the test solution, between samples S7 and S6.

In Fig. 14(a), the impedance spectra shows only one capacitive contribution, with impedance values, at low frequency, on the order of $2 \times 10^4\ \Omega cm^2$, i.e., one order of magnitude larger than the other samples. After 1 day of exposure, there is a trend for the value to decrease, and after 5 days of exposure, a value on order of $4 \times 10^3\ \Omega cm^2$ was observed. Fig. 14(b), shows one time constant with maximum around 70 °, that after one day of exposure, shifted to lower frequencies with a maximum of about 68 °. A clear evidence of the beneficial effect of the N_2/Ar flow rate is observed by comparing the phase angle values at time 0 of Figs. 13 and 14. The highest values observed in the latter case suggest the major stability and the superior dielectric properties of the film formed on the surface of sample S8.

Qualitatively sample S8 presents the highest corrosion protection followed by S7, S6, S5 and S1, respectively. This behaviour is in agreement with the results obtained from the polarisation curves.

The E_{corr} values become nobler during exposure in the test solution. This phenomenon is certainly due to nitriding of the

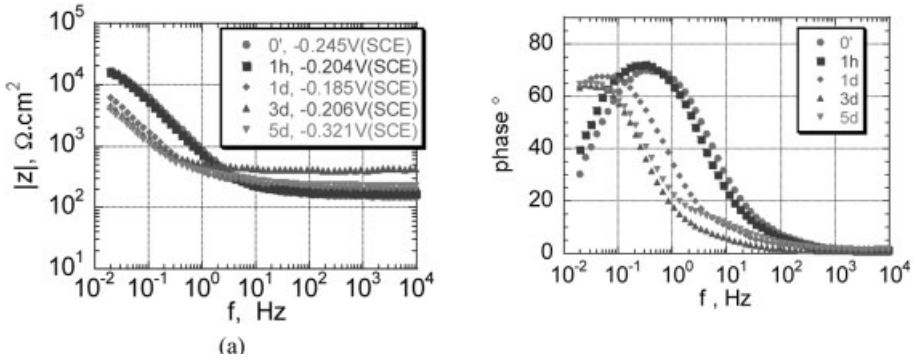

Fig. 14. Bode plot (a) and phase angle (b) as a function of immersion time in aqueous aerated 0.6N NaCl solution at pH 12, for MoN_x sample, with x = 1.0 (S8)

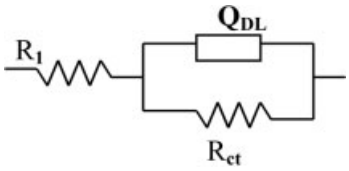

Fig. 15. Equivalent circuit employed during the current research

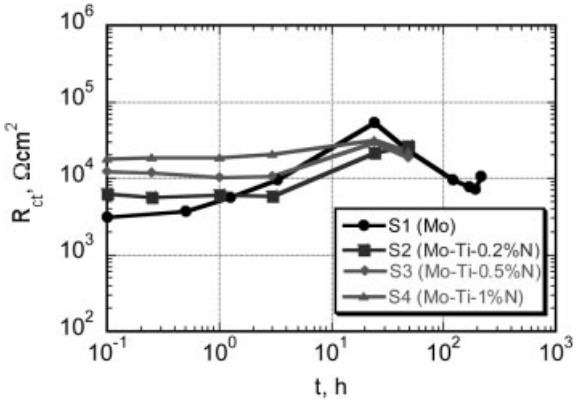

Fig. 16. Values of R_{ct} as a function of immersion time in aerated 0.6N NaCl solution, obtained from ZView for pure molybdenum and Mo-Ti nitride thin film samples

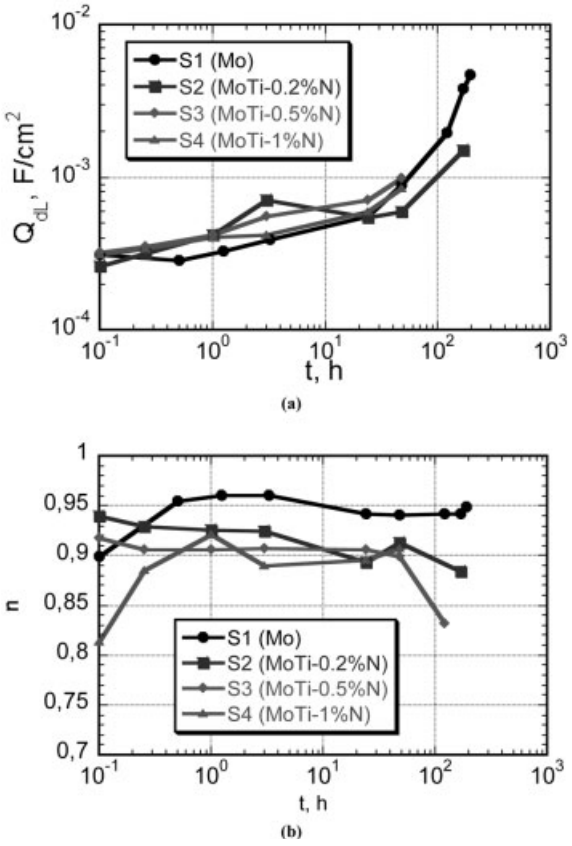

Fig. 17. Values of Q_{dl} and n as a function of immersion time in aerated 0.6N NaCl solution, obtained from ZView for pure molybdenum and Mo-Ti nitride thin film samples

upper surface of the samples occurring during sputtering in the nitrogen, that forms a passive film on the sample surface.

3.3 Equivalent spectra

The experimental impedance spectra, shown in Figs. 7 to 14 were analysed on the basis of the equivalent electric circuit presented in Fig. 15 [30], using the ZView software from Scribner Associates. The R_1 is the resistance of the film plus the resistance of the external electrolyte, R_{ct} is the charge transfer resistance, and Q_{dl} is the double layer capacitance. The capacitor Q_{dl} is mathematically modelled using constant-phase elements (CPE) [31].

The comparison between the simulated and experimental data at different stages of exposure is omitted for simplicity, however, in all cases, the experimental data are in good agreement with model predictions at every exposure time.

The values of R_{ct}, Q_{dl} and n, obtained in aqueous aerated 0.6N NaCl solution at pH 12, for MoTi nitride thin film samples, were reported in Figs. 16 and 17. The pure molybdenum was used as a standard reference sample.

Fig. 16 presents values of R_{ct} as a function of immersion time in the test solution for pure molybdenum as well as for the MoTiN thin film samples. It is apparent from this figure that the R_{ct} value at time zero for sample S1 is about $3 \times 10^3\ \Omega cm^2$. The Mo sample exhibits low stability with the corrosion rate decreasing during the first day, but subsequently exhibits an increasing rate during most of the remainder of the test. Conversely, the MoTiN samples exhibit a more stable corrosion rate, with the stability increasing as a function of increasing nitrogen flow.

Further, the MoTiN samples exhibit short term R_{ct} values that increase as a function of increasing N_2/Ar flow rate. This result suggests the formation of a more stable surface barrier layer in the latter case.

Figs. 17(a) and 17(b) show values of Q_{dl} and its coefficients, n, as a function of immersion time in the test solution for the

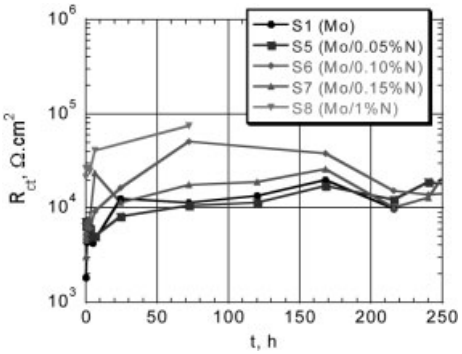

Fig. 18. Values of R_{ct} as a function of immersion time in aerated 0.6N NaCl solution, obtained from ZView for pure molybdenum and molybdenum nitride thin film samples

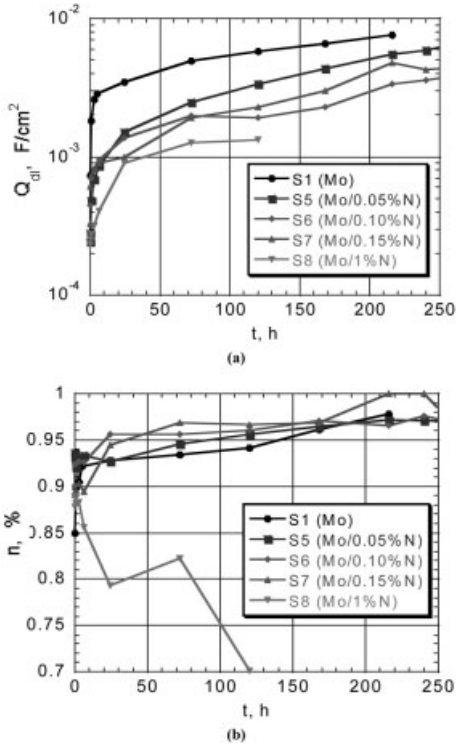

Fig. 19. Values of Q_{dl} and n as a function of immersion time in aerated 0.6N NaCl solution, obtained from ZView for pure molybdenum and molybdenum nitride thin film samples

pure molybdenum and for the MoTiN thin film samples. It can be observed that, in all cases, the Q_{dl} increases with exposure time. This behaviour indicates degradation of the film during the exposure period. In Fig. 17(b) the n values are between approximately 0.9 and 0.95.

The values of R_{ct}, Q_{dl} and n, obtained in aqueous aerated 0.6N NaCl solution at pH 12, for molybdenum nitride thin film samples, are reported in Figs. 18 to 19. Pure molybdenum was used as a reference.

Fig. 18 reveals values of R_{ct} as a function of immersion time, obtained in the test solution. The S1 and S5 samples show similar behaviour and the S8 sample has the highest charge transfer resistance values in comparison to the others, suggesting better corrosion resistance.

Figs. 19(a) and (b) present values of Q_{dl} and n as a function of immersion time, obtained in aqueous aerated chloride solution at pH 12. The behaviour of Q_{dl} that can be correlated to the alloys stability, further corroborates the superior behaviour of sample S8.

4 Conclusions

Based on the results generated during this investigation on MoN and MoTiN thin film samples, the following conclusions can be drawn:

Increasing of the N_2/Ar flow ratio in the deposition process induces:

- a decrease in deposition efficiency (higher sheet resistance and lower thickness);
- a more noble corrosion potential;
- a decrease of the kinetics of electrochemical reactions;

The electrochemical techniques (polarisation curves and EIS measurements) are useful tools for characterization and evaluation of corrosion behaviour of the MoN and MoTiN thin film samples examined during this study.

The EIS data analysis based on the equivalent electrical circuit indicates that samples S8 exhibits better corrosion protection, which is confirmed by the dc electrochemical behaviour.

Finally, the deposition in the highest N_2/Ar flow rate produces both high corrosion resistance and low electrical conductivity of the film. This could result in a higher stability of the layer but also in a lower efficiency of the back contact.

5 Acknowledgements

The authors gratefully acknowledge the support given by the European Commission under contract ERK6-CT1999-0009.

6 References

[1] D. D. Bacon, A. T. English, S. Nakahara, F. G. Peters, H. Schreiber, W. R. Sinclair, R. B. Van Dover, *J. Appl. Phys.* **1983**, *54*, 6509.
[2] R. Fix, R. G. Gordon, D. M. Hoffman, *Thin Solid Films* **1996**, *288*, 116.
[3] N. Solak, F. Ustel, M. Urgen, S. Aydin, A. F. Cakir, *Surf. Coat. Technol.* **2003**, *174–175*, 713.
[4] M. Urgen, O. L. Eryilmaz, A. F. Çakir, E. S. Kayali, B. Nilüfer, Y. Isik, *Surf. Coat. Technol.* **1997**, *94*, 501.
[5] I. Jauberteau, J. L. Jauberteau, M. N. Semeria, A. Larre, J. Piaguet, J. Aubreton, *Surf. Coat. Technol.* **1999**, *116–119*, 222.
[6] S. Konstantinidis, C. Nouvellon, J.-P. Dauchot, M. Wautelet, M. Hecq, *Surf. Coat. Technol.* **2003**, *174–175*, 100.
[7] V. P. Anitha, A. Bhattacharya, N. G. Patil, S. Major, *Thin Solid Films* **1993**, *236*, 306.
[8] V. P. Anitha, S. Major, D. Chandrashekharam, M. Bhatnagar, *Surf. Coat. Technol.* **1996**, *79*, 50.
[9] P. J. Kelly, R. D. Arnell, *Vacuum* **2000**, *56*, 159.
[10] J. D. Wu, C. Z. Wu, Z. M. Song, F. M. Li, *Thin Solid Films* **1997**, *311*, 62.
[11] J. D. Wu, C. Z. Wu, Z. M. Song, L. H. Wu, F. M. Li, *Appl. Surf. Sci.* **1995**, *90*, 81.
[12] R. Martínez, J. A. García, R .J. Rodríguez, B. Lerga, C. Labrugère, M. Lahaye, A. Guette, *Surf. Coat. Technol.* **2003**, *174–175*, 1253.
[13] S. Hoffmann, *Thin Solid Films* **1990**, *191*, 335.
[14] D. A. Papaconstantopoulos, W. E. Pickett, B. M. Klein, L. L. Boyer, *Phys. Rev. B* **1985**, *31*, 752.
[15] H. Ihara, M. Hirabayashi, K. Senzaki, Y. Kimura, H. Kezuka, *Phys. Rev. B* **1985**, *32*, 1816.

[16] E. P. Donovan, G. K. Hubler, M. S. Mudholkar, L. L. Thompson, *Surf. Coat. Technol.* **1994**, *66*, 499.
[17] J. Valli, U. Mäkelä, H. T. G. Hentzell, *J. Vac. Sci. Technol.* **1986**, *4*, 2850.
[18] J. E. Truman, M. J. Coleman, K. R. Pirt, *Br. Corr. J.* **1977**, *12*, 236.
[19] S. Maximovitch, G. Barral, F. Le Cras, F. Claudet, *Corr. Sci.* **1995**, *37*, 271.
[20] G. O. Ilevbare, G. T. Burstein, *Corr. Sci.* **2001**, *43*, 485.
[21] F. Lévy, P. Hones, P. E. Schmid, R. SanjinÄs, M. Diserens, C. Wiemer, *Surf. Coat. Technol.* **1999**, *120–121*, 284.
[22] V. P. Anitha, S. Vitta, S. Major, *Thin Solid Films* **1994**, *245*, 1.
[23] Y. C. Lu, M. B. Ives, *Corr. Sci.* **1992**, *33*, 317.
[24] M. Nagae, S. Okada, M. Nakanishi, J. Takada, Y. Hiraoka, Y. Takemoto, M. Hida, H. Kuwahara, M. K. Yoo, *International Journal of Refractory Metals Materials* **1998**, *16*, 127 .
[25] L. De Rosa, C. R. Tomachuk, J. Springer, D. B. Mitton, S. Saiello, F. Bellucci, *Materials and Corrosion* **2003**, *55*, 602.
[26] C. R. Tomachuk, L. De Rosa, J. Springer, D. B. Mitton, S. Saiello, F. Bellucci, *Materials and Corrosion* **2003**, *55*, 665.
[27] R. Mientus, K. Ellmer, *Surf. Coat. Technol.* **1999**, *116–119*, 1093.
[28] J. W. Johnson, C. H. Chi, C. K. Chen, W. J. James, *Corrosion* **1970**, *26*, 238.
[29] F. Mansfeld, *J. Appl. Electrochem.* **1995**, *25*, 187.
[30] W. A. Badaway, F. M. Al-Kharafi, *Electrochim. Acta* **1998**, *44*, 693.
[31] B. A. Boukamp, *Solid State Ionics* **1977**, *20*, 31.

(Received: July 11, 2005) W 3939